Robotica (2013) volume 31, pp. 441–453. © Cambridge University Press 2012
doi:10.1017/S026357471200046X

A reconfigurable, tendon-based haptic interface for research into human-environment interactions

Joachim von Zitzewitz†,‡,* André Morger†, Georg Rauter†, Laura Marchal-Crespo†, Francesco Crivelli†, Dario Wyss†, Tobias Bruckmann§ and Robert Riener†,¶

†*Sensory-Motor Systems (SMS) Lab, Institute of Robotics and Intelligent Systems (IRIS), ETH Zurich, 8092 Zurich, Switzerland*
‡*Brain Mind Institute, EPFL Lausanne, 1015 Lausanne, Switzerland*
§*Chair for Mechatronics, University Duisburg-Essen, 47057 Duisburg, Germany*
¶*Medical Faculty, University of Zurich, 8092 Zurich, Switzerland*

(Accepted July 18, 2012. First published online: August 14, 2012)

SUMMARY
Human reaction to external stimuli can be investigated in a comprehensive way by using a versatile virtual-reality setup involving multiple display technologies. It is apparent that versatility remains a main challenge when human reactions are examined through the use of haptic interfaces as the interfaces must be able to cope with the entire range of diverse movements and forces/torques a human subject produces. To address the versatility challenge, we have developed a large-scale reconfigurable tendon-based haptic interface which can be adapted to a large variety of task dynamics and is integrated into a Cave Automatic Virtual Environment (CAVE). To prove the versatility of the haptic interface, two tasks, incorporating once the force and once the velocity extrema of a human subject's extremities, were implemented: a simulator with 3-DOF highly dynamic force feedback and a 3-DOF setup optimized to perform dynamic movements. In addition, a 6-DOF platform capable of lifting a human subject off the ground was realized. For these three applications, a position controller was implemented, adapted to each task, and tested. In the controller tests with highly different, task-specific trajectories, the three robot configurations fulfilled the demands on the application-specific accuracy which illustrates and confirms the versatility of the developed haptic interface.

KEYWORDS: Haptic interfaces; Parallel manipulators; Design; Man–machine systems; Control of robotic systems.

1. Introduction

1.1. A versatile haptic interface for systematic research on human-environment interaction

Haptic interfaces offer new possibilities to explore the interaction between a human subject and his environment. Recent developments in robotics on both, the control and the hardware side significantly augment the possibility to provide multi-dimensional, high-quality force rendering and feedback to a human subject.[1-3]

To optimize the control of these haptic interfaces and the other rendering and feedback modalities involved in the virtual-reality (VR) scenario such as visual and acoustic displays, the general "human-in-the-loop" question[4] is of great interest: In which way can changes in the (virtual) environment provoke desired reactions of the human? The hypothesis can be formulated that similar feedback principles can be applied to different multi-modal VR setups in order to influence a test subject's reaction in a targeted and predictable way.

To investigate these principles systematically, we need a versatile, highly adaptable multi-modal VR-setup. A "perfect" setup should allow to investigate a wide range of applications with the same methodology in order to obtain generalizable results. Herein, the required versatility/adaptability also refers to the haptic modality.

To answer the human-in-the-loop question, the reaction of the human nervous system to the virtual scenarios is of interest.[5] Activities under conscious control (focusing on the central nervous system and, more specifically, on the sensory-motor system) and autonomous, unconscious body activities (focusing on the peripheral nervous system) can be differentiated in the human nervous system.[6]

Research on the sensory-motor system can be ideally performed in the field of motor learning in sports. In an internal review on different kinds of sports, racket and net sports like tennis or baseball were found to be the motion group with the highest end-effector velocities on the upper extremity and the end effector.[7-9] Concerning sports involving repetitive whole-body movements, rowing was found to be a sport with elevated peak power and peak force of up to 1.2 kW and 800 N, respectively.[9-11] Therefore, tennis and rowing were chosen as sports which describe the limits of the required spectrum of dynamics. The dynamical requirements for research on the unconscious body activities are similar. Additional side requirements might emerge, however, e.g., minimal noise emission in the special case of sleep research. In summary, a robotic system, which is

* Corresponding author. E-mail: joachim.vonzitzewitz@epfl.ch

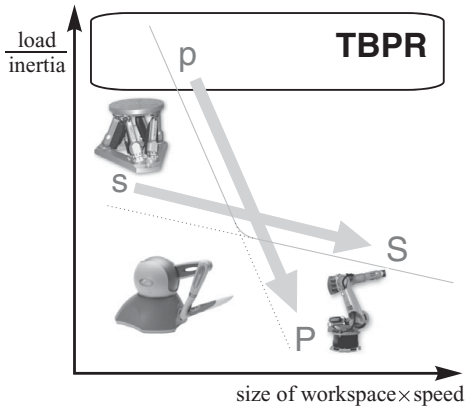

Fig. 1. Load-to-inertia ratio of different robot types with respect to workspace size and maximal speed (*p*: small parallel robot, P: large parallel robot, s: small serial robot, S: large serial robot, TBPR: tendon-based parallel robot).

capable of fulfilling the requirements of motor learning in rowing and tennis on one hand and of sleep research on the other hand, offers optimal conditions to globally address research on the reaction of the human nervous system to external stimuli.

1.2. Use and limitations of haptic interfaces

Haptic displays enable realistic and repetitive training of tasks in a safe environment, e.g., in medical training, in flight simulators, and in robot-assisted rehabilitation. As tools for teleoperation, they provide haptic feedback or tactile information about environments which the operator cannot reach directly.

A large number of serial robots and parallel robots with rigid links are used as haptic displays. The Phantom device[12] and the Delta Haptic Interface[13] are prominent and commercially available examples with serial and parallel structures, respectively. Each robot structure has different advantages and disadvantages: Generally, parallel robots are characterized, for example, by a high load-to-inertia ratio, whereas serial robots cover a larger workspace. In general, both types with rigid links are disadvantageous in large-scale environments, as an increase in workspace leads to an increase of inertial mass (Fig. 1). As this inertia is at least partially felt by the user when actively accelerating the device,[14] the transparency of the haptic interface decreases with an increase in workspace size. This disadvantage does not apply to one subgroup of parallel robots: Tendon-based robots have inertial properties which are almost independent of their size. The arms of tendon-based robots only consist of lightweight tendons connected in parallel to the end effector. The main inertial part is the motorized drum to wind up the rope.

1.3. A reconfigurable rope robot used as a versatile large-scale haptic interface

The high variety of load cases and task-specific workspace shapes emerging from the research goals formulated in Section 1.1 cannot be realized with a single fixed robotic structure but requires a reconfigurable robot. This requirement for reconfigurability and the use of multiple feedback modalities, which should not be influenced by the robot, favor the use of an intrinsically modular tendon-based system.

During the last years, we have developed a tendon-based system, the so-called r^3-system (**r**econfigurable **r**ope **r**obot) as a haptic interface with versatile capabilities embedded in a CAVE (Cave Automatic Virtual Environment) setup.[15] A major goal of this project was that hardware and software components of the robot should be applicable for different applications to facilitate the fast adaptation of the system to new tasks.

This paper will present the robot design as well as three applications reflecting the versatility of the system. It describes the underlying concept for model-based position control, as well as the application-specific adaptations of the hardware and the controller. Finally, the performance of the controller will be evaluated in order to prove that the control performance satisfies the versatile, task-specific requirements.

2. Setup of the r^3-System

2.1. Requirements

After the required robot type, a tendon-based system, is derived from the tasks and the environmental conditions, the more detailed technical requirements of the robot axes must be defined.

The r^3-system has to fulfill the general technical requirements of haptic displays: To achieve realistic rendering of hard surfaces, smooth velocity measurements with small computational delay are required.[16] To fulfill these requirements, a sampling frequency of about 1 kHz[17] and a minimal position resolution of 1.25 µm[18] are suggested as sufficiently high. In addition, the haptic display has to be backdrivable for safety reasons[19] and to enable motion-driven control strategies.[20] Nevertheless, a subset of axes should be optionally lockable in case of emergency shutdown, e.g., to prevent a person from falling when he/she is lifted with the robot.

Furthermore, the robot has to be able to cope with the high dynamics required for sports simulation, mainly in terms of force and velocity. Therefore, the maximal values for these parameters were extracted from the literature: In tennis, racket velocities can reach values of up to 37.5 m/s.[9] Maximal peak hand forces occur in rowing and can reach up to 800 N. With a user-cooperative robot capable of producing these dynamics, a large variety of sports can be simulated.

However, these values do not necessarily correspond with the requirements on a single robot axis. In tendon-based robots, end-effector velocity in specific workspace areas and directions can become more than three times larger than the velocity of a single axis depending on the robot configuration.[21] Equivalently, the end-effector force can exceed the payload of a single axis by an approximated factor of 1.5. Given these task dynamics and the amplification factors, the maximal velocity and the peak force of a drive train can be roughly approximated as 12 m/s and 500 N, respectively, without taking a safety factor into consideration.

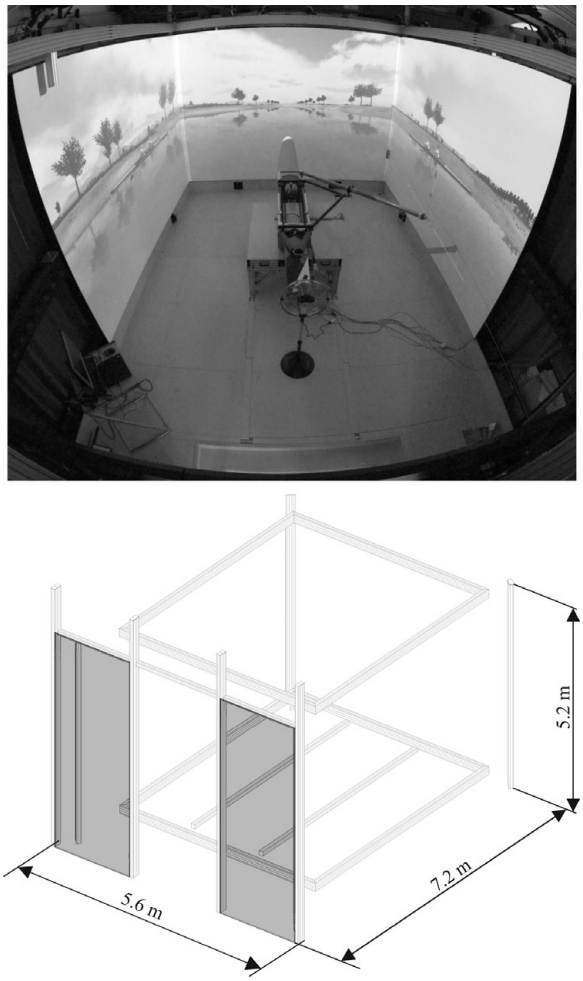

Fig. 2. Frame structure of the r^3-system (below) surrounding the CAVE (above); only the frame parts are depicted, where deflection units can be mounted (including the grey area).

As mentioned above, the r^3-system is integrated into a CAVE. Inside this CAVE, the user's workspace has a maximum length of 4.5 m. This value was defined as the minimal rope length which can be wound up on a single axis. Moreover, the haptic display should not disturb the other modalities of the CAVE, such as the acoustic and the visual displays, in order to achieve realistic multi-modal rendering of the task.

2.2. Frame structure

In tendon-based robots, a frame structure surrounds the workspace. From this frame, the ropes are guided directly from the motorized axes or via deflection units to the end effector.

The frame structure of the r^3-system consists of a modular profile system (Basic Mechanic Elements, Bosch Rexroth, Lohr a.M., Germany). The frame surrounds the entire CAVE. It has a longitudinal extension of 7.2 m, a lateral extension of 5.6 m, and a height of 5.2 m (Fig. 2).

2.3. Mechanical setup

One end of the rope is connected to the end effector. The other end leading, out of the CAVE, is connected to one of the following three types of units (Fig. 3):

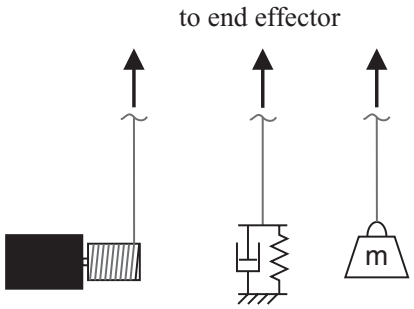

Fig. 3. Active or passive units driving the r^3-system.

- active unit (motorized drums)
- passive unit storing potential energy (e.g., a mass or a spring)
- passive unit dissipating energy (e.g., a brake)

The active units (the motorized drums) of the r^3-system are mounted on the ground in the lower corners of the frame. Each active unit comprises a drum actuated by an AC-servo motor (AKM53G, Danaher, Pennsylvania, USA). An electromagnetic safety brake can block the drum when the power supply of the robot is switched off. From each drive train, the rope is guided into the workspace via a tensionmeter and a deflection unit.[22]

The current robot setup comprises seven axes. To adapt the transmission ratio on each axis to tasks with different force-torque/velocity profiles, the drum diameter of the drive trains can be chosen between 75 and 150 mm. The drums are mounted on the outer end of the axis to facilitate their replacement.[22] The range of the adaptable transmission ratio can be augmented by applying the tackle principle as also proposed by Merlet.[23] A single axis has a nominal power of 2 kW, a continuous payload of 262 N and a peak payload of 790 N, both with the smallest drum mounted. With the largest drum mounted, a velocity of 16 m/s can be reached.

2.4. Deflection unit

The deflection units (Fig. 4) can be mounted at arbitrary positions on the frame structure of the robot (Fig. 2). They guide the rope into the workspace between two pulleys and two rollers. Optionally, a plate with a U-bolt can be mounted on the deflection unit. The free end of the rope deflected at the end effector can be fixed to this U-bolt, if the tackle principle is applied. A more detailed description of the deflection units, including the geometrical modeling, can be found in a preceding paper.[24]

2.5. Sensor setup

Each axis is equipped with three sensors: one encoder attached to the motor shaft, one analog position measurement unit (APMU) that measures the absolute drum angle, and one analog force sensor (tensionmeter).

The encoder on the motor shaft is an absolute 20-bit single turn encoder. The resulting maximal linear resolution is 0.5 µm for a single axis with the smallest drum.

The main requirement for the APMU was a measurement range of 20 revolutions needed to wind up the required rope length of 4.5 m with the smallest drum. This criterion

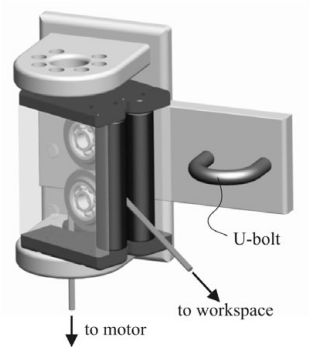

Fig. 4. Deflection unit of the r^3-system.

was fulfilled by using a wire potentiometer whose wire is wound up on a thread mounted at the end of a motor axis. The availability of the absolute motor position makes a re-calibration of the robot after a system shut-down dispensable.[22] Furthermore, the redundant measurement of the motor position serves as a safety feature, as for example proposed by Bouri *et al.*[25] Using the analogue wire potentiometer, the proper function of the digital encoder measurement can be continuously supervised.

As the third sensor type, tensionmeters are integrated on each axis to measure the rope force.[22] The tensionmeters have a nominal load of 1000 N and a non-linearity of 0.3 %. They are mounted on the frame structure and placed between the motorized winches and the deflection units which guide the rope into the workspace. This stationary solution facilitates wiring and, hence, promotes the modularity of the system compared to force sensors connected to the end effector.[26] The disadvantage of this solution is that the rope force is not measured directly at the end effector, but before the deflection unit. The rope is wound around a pulley mounted on the tensionmeters. As the accuracy and resolution of the sensor increase with the deflection angle around this pulley, the deflection angle should be maximized. The deflection angle is 90° if the deflection unit is mounted on the upper part of the frame, and 52°, if the deflection unit is mounted on the floor.

2.6. Signal processing

Signal processing has a large impact on the quality of a haptic interface. Signal noise and time delays should be reduced to a minimum, and the sampling frequency and resolution of the sensor signals have to fulfill the high requirements listed in Section 2.1.

We decided to implement the digital communication protocol EtherCAT (Ethernet for Control Automation Technology).[27] This protocol has the advantage of high scalability, i.e., additional channels can be added to hard- and software with little effort, and it is implemented in the motor drives of several suppliers.

With this protocol, the analog signals can be digitized by so-called EtherCAT-terminals (Beckhoff, Verl, Germany) with a conversion time of approximately 60 µs. As this digitalization takes place close to the analog sensors, their cable length and thus signal noise are reduced.

Except for the encoder cables, which directly connect the motors and the motor drives, all sensor signals are transmitted via a single network cable connecting the terminals in the corners of the CAVE. Also the motor drives (S700, Danaher, Pennsylvania, USA) are addressed via EtherCAT. Additional sensors needed inside the CAVE for specific applications, e.g., a rowing simulator,[28] are digitized by further terminals connected to the EtherCAT net.

The preferred programming software was Matlab/Simulink in combination with an xPC real-time target computer. As Simulink/xPC (Matlab version 2009b) cannot handle the EtherCAT protocol, a real time Linux-PC was used. This PC runs custom software that acts as a gateway between the EtherCAT network and the xPC-target. The Linux computer and the xPC-target communicate via Raw Ethernet. The Linux-PC clocks the xPC-target with parallel port interrupts. Synchronization between the two computers is secured by redundant transmission of time information over the parallel port and Ethernet (Fig. 5). The control program runs at a cycle times of 0.25 ms.

2.7. Supplementary setup: Optical tracking

An opto-electronic motion tracking system (Qualisys, Gothenburg, Sweden) is installed around the CAVE. Up to 10 cameras are used to detect the position of passive markers fixed to the robot or the user. The marker positions are transmitted via UDP to the xPC-target at a frequency of 200 Hz.

3. Model-based Position Control

Not only hardware but also software components should be reusable or easily adaptable for different applications. The complete reusability of all software components and control strategy for all tasks is not necessarily possible, as shown in the following sections. While standard approaches may satisfy the requirements of some tasks, they might require more or less laborious extensions for others.

In addition, the definition of a research goal often makes the development of very specific control approaches necessary. In this context, advanced force control strategies have already been implemented in the system, e.g., for research on different support strategies in motor learning.[29]

But these specific strategies are not the focus of this paper. Its aim is rather to present a (basic) control strategy illustrating the comments above. The only control strategy implementable in all three applications realized up to now is position control. As already mentioned, one major research focus in the M3-Lab is robot supported motor learning. In this context, position control can be regarded as the simplest assistive control strategy usable to guide a user along a specific trajectory, e.g., for teaching purposes. Furthermore, a reliable position controller often serves as a basis for several user-cooperative control strategies such as admittance control[30] or open-loop impedance control.[31]

The focus is put on the control performance of the proper robot, because position tracking of the robot (effective vs. measured robot position) has been evaluated elsewhere.[24]

3.1. Basic control concept

As a basis for more advanced control strategies, a well-known control approach was chosen: A proportional-derivative (PD) computed-torque controller was implemented to control

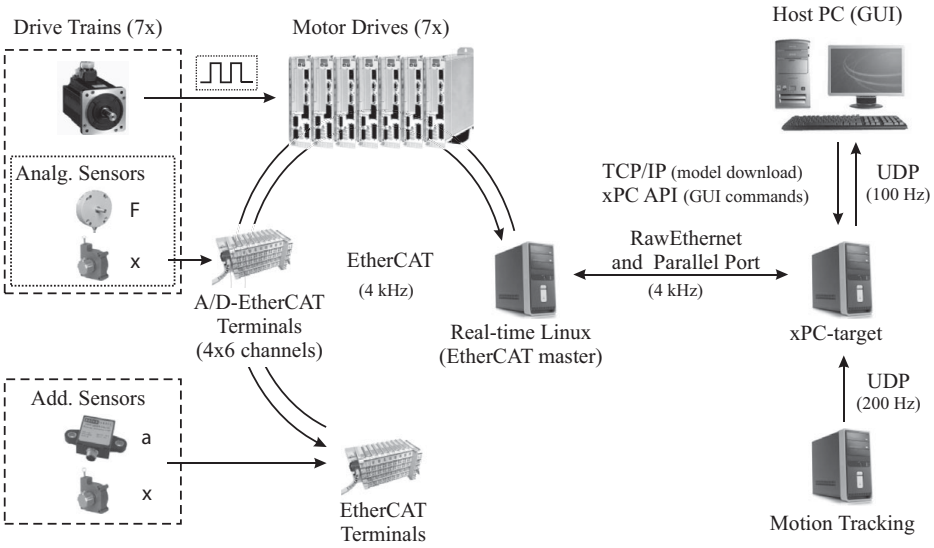

Fig. 5. Signal processing flow chart of the r^3-system.

the pose (position and orientation) of the end-effector in task space. A task-space controller was chosen due to its superior properties concerning accuracy and interactive control compared to joint-space controllers.[32] Furthermore, this control approach can easily be extended by further modules for improved performance in case it does not satisfy the task requirements, as will be shown later.

The actual end-effector pose $\boldsymbol{x}_{EE}$ is derived from the measured rope lengths $\boldsymbol{l}_m$ by a physics-based approach for forward kinematics.[24] Using the inverse robot model, the external forces and torques acting on the end effector, namely gravity, friction, and inertia are modeled and compensated. This modeled external wrench is summarized in $\hat{\boldsymbol{w}}$ (Fig. 6). The total commanded wrench $\boldsymbol{w}_c$ is subdivided into single rope forces $\boldsymbol{f}_c$ using a quadratic programming (QP) approach.[33] This approach guarantees continuity of the single rope forces while rope forces are minimized.[34] The minimal and maximal rope forces can be defined as inequality constraints of the quadratic program.

3.2. Inverse robot model

To calculate the feed-forward part for model-based control strategies, the inverse robot model is required. The input of the inverse model is the desired pose $\boldsymbol{x}_{EE,d}$ of the robot and its derivatives; the output is the modeled wrench $\hat{\boldsymbol{w}}$. In tendon-based robots, it is advantageous to split the inverse model into two parts: the drive-train model (output wrench $\hat{\boldsymbol{w}}_{DT}$) and the end-effector model (output wrench $\hat{\boldsymbol{w}}_{EE}$).

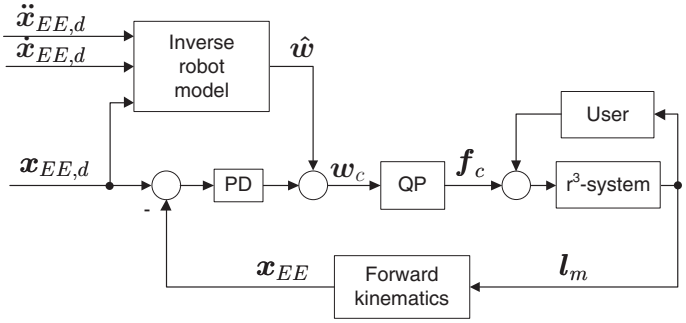

Fig. 6. Computed-torque position controller of the r^3-system ($\boldsymbol{x}_{EE,d}$: desired end-effector position, $\boldsymbol{x}_{EE}$: actual end-effector position, $\hat{\boldsymbol{w}}$: modeled wrench, $\boldsymbol{w}_c$: commanded wrench, $\boldsymbol{f}_c$: commanded rope forces, $\boldsymbol{l}_m$: measured rope lengths, QP: quadratic optimizer).

The drive-train model accounts for inertial and friction effects of the drive train summarized in the torque vectors $\hat{\boldsymbol{\tau}}_{\boldsymbol{I}}$ and $\hat{\boldsymbol{\tau}}_{\boldsymbol{f}}$, respectively; it is driven by motor angles $\boldsymbol{\varphi}_m$ and their derivatives. The motor angles are obtained from the inverse kinematics[32] which transforms $\dot{\boldsymbol{x}}_{EE,d}$ and $\ddot{\boldsymbol{x}}_{EE,d}$ into rope velocity $\dot{\boldsymbol{l}}$ and rope acceleration $\ddot{\boldsymbol{l}}$. The approximated angular velocity and acceleration of the motor, $\hat{\dot{\boldsymbol{\varphi}}}_{\boldsymbol{M}}$ and $\hat{\ddot{\boldsymbol{\varphi}}}_{\boldsymbol{M}}$, respectively, are calculated from the rope movement by division by the drum radius r_D (Fig. 7). The modeled wrench of the drive train $\hat{\boldsymbol{w}}_{DT}$ is calculated as

$$\hat{\boldsymbol{w}}_{DT} = \underbrace{\begin{bmatrix} \boldsymbol{v}_1 & \dots & \boldsymbol{v}_m \\ \boldsymbol{p}_1 \times \boldsymbol{v}_1 & \dots & \boldsymbol{p}_m \times \boldsymbol{v}_m \end{bmatrix}}_{\mathbf{A}^T} \cdot \frac{1}{r_D}(\hat{\boldsymbol{\tau}}_{\boldsymbol{I}} + \hat{\boldsymbol{\tau}}_{\boldsymbol{f}}) \qquad (1)$$

with $\mathbf{A}^T$ as the structure matrix of the rope robot; the vector $\boldsymbol{v}_i$ is the unit vector in the direction of the ith rope, $\boldsymbol{p}_i$ is the vector from the origin of the end effector to the i-th connection point, and m is the number of ropes.

The moment of inertia of the motorized drum J_O required to calculate $\hat{\boldsymbol{\tau}}_{\boldsymbol{I}}$ can be extracted from CAD and data sheets. The friction model was derived experimentally as further described in Section 3.3.

If the end effector consists of a single body attached to the ropes, the corresponding models can be found in the literature[32] and are, therefore, not further treated in this paper. However, the model might require further application-dependent adaptations, as will be shown later in Section 4.3.

3.3. Friction model

The friction of the r^3-system, including the motor unit, the deflection unit, and the pulley at the force sensor, was determined experimentally. Therefore, the rope was guided vertically into the workspace where it was attached to a test

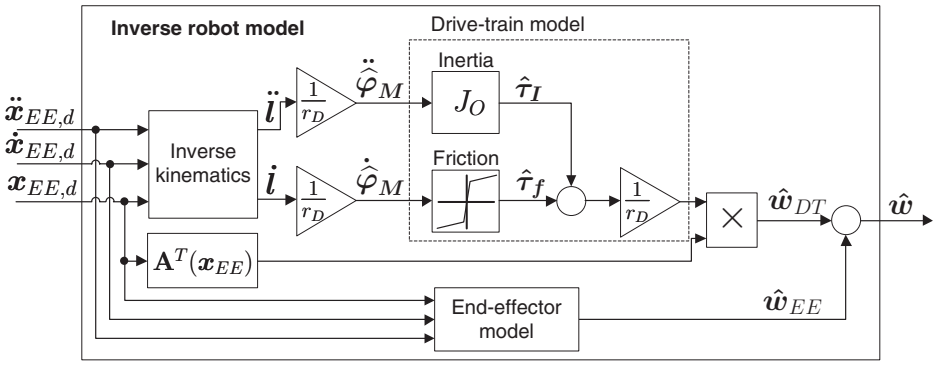

Fig. 7. Flow chart of the inverse robot model.

mass m_t of 10 kg standing on the ground. A torque ramp was set to the motor. At a certain point, the mass started to move upwards. The motor automatically stopped when the mass reached a defined height. The motor angle φ_m, the force at the tensionmeter f_m, as well as the commanded torque τ_{cmd} were recorded. The torque resulting from the friction of the drive train can consequently be calculated as

$$\tau_f = \tau_{cmd} - J_O \cdot \ddot{\varphi}_m - (m_t \cdot (g + \ddot{\varphi}_m \cdot r_D)) \cdot r_D. \quad (2)$$

As the tensionmeter is placed between the motor and the deflection unit, the motor torque necessary to overcome the friction of the deflection unit $\tau_{f,DU}$ can be derived from the measured rope force as

$$\tau_{f,DU} = (f_m - m_t \cdot (g + \ddot{\varphi}_m \cdot r_D)) \cdot r_D. \quad (3)$$

For model-based friction compensation, the obtained curve was approximated by two intersecting linear functions.

4. Three Applications Realized with the r³-System

The versatility of the r³-system is illustrated by three different applications. As an example for a setup for haptic rendering involving high interaction forces, a rowing simulator is presented below. This simulator is capable of rendering forces at an oar blade depending on the user's movement. As a further 3D task, a training tool for a tennis stroke providing haptic guidance during highly dynamic movements will be presented. A third example will explain a 6D platform capable of lifting the user from the ground.

4.1. Rowing simulator with 3D haptic feedback

To fulfill the requirements of this first project, the r³-system has to cope with the combination of dynamic movements and dynamic loads including high peak loads as they occur in rowing: The aim of this project was to develop an advanced rowing simulator including visual, auditory, and haptic feedback. The r³-system should not only be able to realistically render oar forces in three dimensions in accordance with the user's movement, it should moreover serve as a teaching tool to provide haptic guidance to the user.

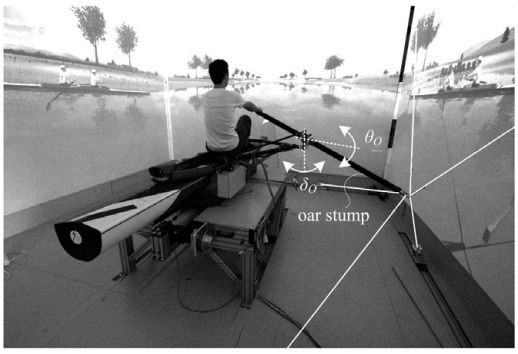

Fig. 8. The rowing simulator with the r³-system to provide haptic feedback.

4.1.1. Setup. Five actuated ropes of the r³-system are connected to a single point on the outer part of an oar stump (Fig. 8). The oar is fixed inside an oar lock of an instrumented shortened scull boat mounted on a podium.[35] The oar lock restricts the oar movement to three rotational degrees of freedom (DOFs): the oar angles in the horizontal and the vertical plane θ_O and δ_O, respectively, can be influenced by the robot while the rotation about the longitudinal oar axis remains a free passive DOF. The diameter of the used winches is 75 mm.

4.1.2. Control of the rowing simulator. Using the position controller, the oar can be guided along a predefined trajectory, e.g., to show the user how to perform a correct rowing movement. The inverse robot model compensates for the dynamics of the drive trains and oar weight. The proportional gain of the controller was set to $P = 2800\,\mathrm{N/m}$, and the derivative gain to $D = 20\,\mathrm{Ns/m}$. The desired position was given in terms of the two controllable oar angles. These oar angles were transformed into cartesian space to obtain the desired end-effector position $\boldsymbol{x}_{des}$.[35] The admissible position error was defined as 1° of the oar's solid angle.

4.1.3. Experimental evaluation. The desired trajectory of the position controller was chosen similar to a typical oar trajectory for moderate rowing:

$$\delta_{O,des}(t) = \frac{15\pi}{180} \sin 0.6\pi t - \frac{10\pi}{180} \quad (4)$$

$$\theta_{O,des}(t) = \frac{40\pi}{180} \cos 0.6\pi t. \quad (5)$$

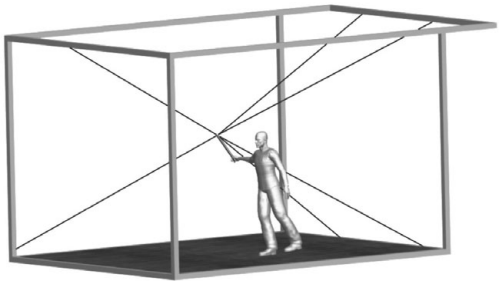

Fig. 9. Configuration of the tennis simulator.

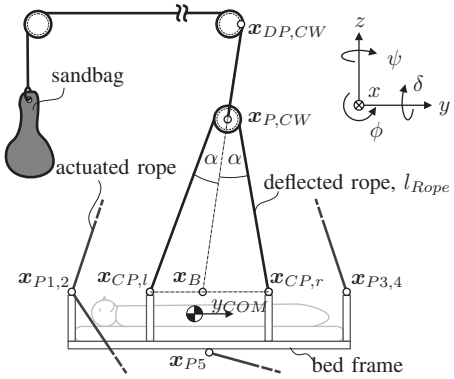

Fig. 10. Fixation of the counterweights (sandbags) to the bed frame (side view).

The actual trajectory of the position controller was measured with and without a user interacting with the oar.[35]

4.2. Training of a dynamic, tennis-like movement

As pointed out in the introduction, a tennis stroke is in the group of highly dynamic movements occurring in sports. We therefore chose to implement a training tool for a tennis-like movement to prove the usability of the robot for user-cooperative tasks involving high end-effector velocities and accelerations. Besides the high dynamics of the tennis movement, the required end-effector workspace close to the user's body is the main difference to the rowing setup.

4.2.1. Setup. The user stands inside the CAVE and holds a racket-like end effector. Six ropes are connected to the end of the racket in a single point (Fig. 9). The user's body movement is restricted by ropes fixed between the robot frame and a climbing harness worn by the user.

4.2.2. Control strategies. The position controller was tested, as it will be used as the simplest assistive controller to teach the movement to the user. The inverse robot model compensated for friction and winch inertia; the proportional gain of the controller was set to $P = 4200\,\mathrm{N/m}$, the derivative gain to $D = 9\,\mathrm{Ns/m}$.

4.2.3. Experimental evaluation. To obtain the reference trajectory for the robotic end effector, a user performed a fast movement with a racket in his hand without being attached to the robot. The trajectory of the racket tip was recorded with the tracking system mentioned in Section 2.7. When using this recorded path as a reference trajectory for the robot, the robot's end-effector moves along an approximately 2.5 m long arc in space reaching a peak velocity of 9.3 m/s. The mean error of the end-effector movement and its standard deviation were evaluated. The admissible error was defined in terms of a timing error of 1 % between actual and desired position. This corresponds to a maximal position error of 5 cm.

4.3. The Somnomat—a 6-DOF platform for vestibular stimulation

In this third application, the capabilities of the r^3-system to cope with high continuous loads was to be investigated. We found an appropriate application in sleep research, where the user has to be entirely lifted from the ground.

The influence of vestibular stimulation on sleep has not been investigated systematically yet. Only studies where seemingly arbitrary movements in a single degree of freedom were used as stimulation can be found.[36-41] To address this topic comprehensively, a device which enables the vestibular stimulation of a sleeping subject in different DOFs without disturbing the subject's sleep, e.g., by noise, is required. Therefore, we configured the robot to manipulate a platform in 6 DOFs, denominated as *Somnomat*.

As a main requirement, the size of the end-effector platform is at least equal to the size of a standard slatted frame and a mattress (0.9×2 m) to have typical conditions for sleep research. The required payload is 105 kg (90 kg as the maximum user weight and 15 kg for additional measurement equipment).

To prevent waking up the subject, pitch and roll angles, ϕ and δ, respectively (Fig. 10), are limited ($\pm 10^\circ$) whereas larger values can be chosen for the yaw (ψ) angle ($\pm 30^\circ$). The desired translational workspace has an extension of ± 0.5 m in all directions.

4.3.1. Setup. Seven actuated ropes are guided to a bed frame structure made of light-weight aluminum profiles: Four ropes coming from the upper part of the frame are connected to the four upper corners of the bed frame ($\boldsymbol{x}_{P1,2,3,4}$ in Fig. 10), and three ropes coming from the ground are connected to the front upper corners ($\boldsymbol{x}_{P1,2}$ in Fig. 10) and to the lower center of the bed frame ($\boldsymbol{x}_{P5}$ in Fig. 10). On all axes, the tackle principle is applied and the smallest winches (diameter of 75 mm) are mounted to cope with the high load. In addition, counterweights in form of sandbags are used to counteract the high static load (Fig. 11). The total counterweight mass is chosen equal to the test subject's mass. The rope of each counterweight is guided into the workspace via the deflection point $\boldsymbol{x}_{DP,CW}$, where it is fixed to a sheave at point $\boldsymbol{x}_{P,CW}$. This sheave runs on a second rope fixed on two points at the upper side of the bed frame (Fig. 10). The total weight of the end-effector platform, including a sleeping subject and measurement equipment, is 153 kg.

4.3.2. End-effector model—counterweight kinematics. As an application-specific solution, the model-based compensation of inertia and weight of the counterweights has to be calculated as a function of the desired end-effector position and acceleration. This leads to a geometrical problem which cannot be solved in a closed form. The basic condition to

solve this problem is that the force on the rope deflected by the sheave is equal on both ends. Consequently, the vector

$$\boldsymbol{v}_{R,CW} = \boldsymbol{x}_{P,CW} - \boldsymbol{x}_{DP,CW} \tag{6}$$

includes the same angle α with the vectors collinear to the two rope ends on the left and right side of the sheave (Fig. 10). Therefore, both of the following two conditions have to be fulfilled:

- The vector from point $\boldsymbol{x}_B$ (intersection between $\boldsymbol{v}_{R,CW}$ and vector described by the connection point of the deflected rope $\boldsymbol{x}_{CP,r}$ and $\boldsymbol{x}_{CP,l}$) to the pulley point $\boldsymbol{x}_{P,CW}$ is collinear with the vector from the pulley to the upper connection point $\boldsymbol{x}_{DP,CW}$.

$$\boldsymbol{x}_{DP,CW} - \boldsymbol{x}_{P,CW} = \lambda \cdot (\boldsymbol{x}_{P,CW} - \boldsymbol{x}_B) \tag{7}$$

- The length of the deflected rope l_{Rope} is constant. The rope is assumed to be deflected around point $\boldsymbol{x}_{P,CW}$ (sheave diameter assumed to be zero):

$$\left|\boldsymbol{x}_{P,CW} - \boldsymbol{x}_{CP,l}\right| + \left|\boldsymbol{x}_{P,CW} - \boldsymbol{x}_{CP,r}\right| = l_{Rope} \tag{8}$$

For the determination of point $\boldsymbol{x}_{P,CW}$, an optimization algorithm is suitable with the argument of minimizing the angular difference between $\boldsymbol{v}_{R,CW}$ and the vectors collinear to the two rope ends on each side of the sheave. To solve the problem, the bisection method is used for the variable $\boldsymbol{x}_B$. At each sampling step of the controller, the point is found by searching in the 10 cm neighborhood of the solution found in the last step. Within 10 iteration steps, the values of $\boldsymbol{x}_B$, and hence the values of $\boldsymbol{x}_{P,CW}$, can be calculated with an accuracy of 0.1 mm. The deflection point $\boldsymbol{x}_{DP,CW}$ is assumed to be a single point.

The second derivative of the sheave position $\boldsymbol{x}_{P,CW}$, however, is too noisy to be used for inertia compensation of the counterweights. The acceleration of the counterweights is, therefore, calculated as if each counterweight rope was directly connected at the intermediate position between $\boldsymbol{x}_{CP,l}$ and $\boldsymbol{x}_{CP,r}$. This approximation is correct for the platform movements which induce large counterweight accelerations, i.e., vertical (z) translations and roll (δ) rotations if the platform is in the central position of the CAVE.

4.3.3. End-effector model—measurement of user position. To warrant the user's safety, his/her position on the platform should be constantly monitored. If the user tries to get up during operation, the system has to stop. Therefore, an online measurement of the user's center of mass $\boldsymbol{x}_{COM}$ on the platform is required. Furthermore, large additional torques are applied to the platform, if the user lies eccentrically in the bed. An online measurement would allow integrating them into the model-based compensation.

The position $\boldsymbol{x}_{COM}$ can be derived from the measured rope forces $\boldsymbol{f}_m$. The measured rope forces $\boldsymbol{f}_m$ have to be transformed from the seven-dimensional joint space to the six-dimensional wrench on the platform by

$$\boldsymbol{w}_{EE,m} = \begin{bmatrix} \boldsymbol{f}_{EE,m} \\ \boldsymbol{\tau}_{EE,m} \end{bmatrix} = \mathbf{A}^T \cdot \boldsymbol{f}_m. \tag{9}$$

To obtain the torque $\boldsymbol{\tau}_{COM}$ resulting from the eccentricity of the center of mass, the model-based end-effector torque $\hat{\boldsymbol{\tau}}_{\boldsymbol{EE}}$ excluding the friction compensation for the motors is subtracted from $\boldsymbol{\tau}_{EE,m}$:

$$\boldsymbol{\tau}_{COM} = \boldsymbol{\tau}_{EE,m} - \hat{\boldsymbol{\tau}}_{EE}. \tag{10}$$

The position of the user on the platform can be calculated by using the first and second element of the vector $\boldsymbol{\tau}_{COM}$ and the platform angles θ and φ:

$$x_{COM} = -\frac{\boldsymbol{\tau}_{COM}(2)}{m_{user} \cdot g \cdot cos(\theta)} \tag{11}$$

$$y_{COM} = -\frac{\boldsymbol{\tau}_{COM}(1)}{m_{user} \cdot g \cdot cos(\varphi)}. \tag{12}$$

4.3.4. Control strategy. As the Somnomat is a comparatively complex setup, model uncertainties are increased. In addition, static control errors gain in importance, because the platform should stay completely horizontal during resting periods. Using the basic control strategy introduced above, the required performance was not achieved anymore. Therefore, it had to be improved and extended.

As with the Somnomat cyclic movements are performed, an iterative learning controller (ILC)[42] was added to the

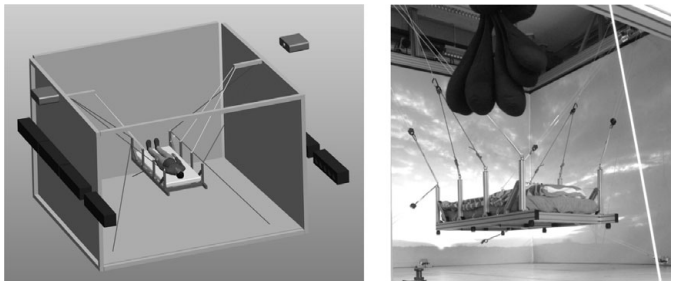

Fig. 11. Setup of the Somnomat; the counterweights (sandbags) are visible in the upper part of the right photo.

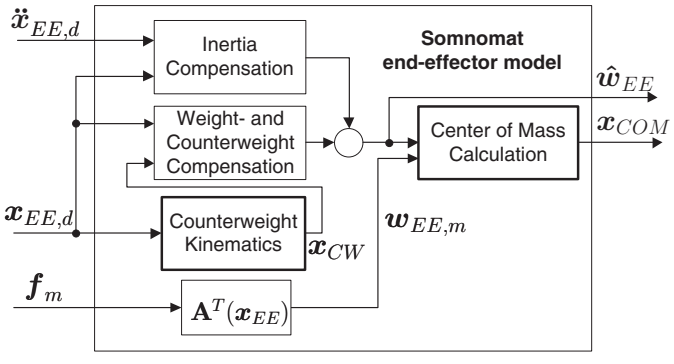

Fig. 12. End-effector model for the Somnomat (bold blocks are further explained in this paper).

control loop to compensate for these uncertainties. This approach was originally developed to optimize controller performance in technical systems operated repeatedly for the same task.[43] This controller takes the control error of a preceding task repetition $k-1$ with the duration interval of $[0; T_f]$ as an input. The output wrench $\bar{\boldsymbol{w}}_k$ is added to the commanded wrench $\boldsymbol{w}_c$ and is calculated as:

$$\bar{\boldsymbol{w}}_k = (1 - f_f) \cdot \bar{\boldsymbol{w}}_{k-1}(t) + \bar{P} \cdot \boldsymbol{e}_{p,i-1}(t) + \bar{D} \cdot \boldsymbol{e}_{v,i-1}(t), t \in [0; T_f], \quad (13)$$

with f_f as a forgetting factor, $\bar{P}$ and $\bar{D}$ as the learning factors for the pose error $\boldsymbol{e}_{p,k-1}$ and velocity error $\boldsymbol{e}_{v,k-1}$ of the previous cycle, respectively.

4.3.5. Evaluation. To evaluate the overall performance of the robot, additional weights of 80 kg were fixed on the mattress. The platform was moved in all DOFs separately at 0.4 Hz with an amplitude of 0.2 m for translational and 0.15 rad (8.6°) for rotational DOFs. Similar trajectories are used for user studies. The admissible position error was defined as 10 mm for the translational DOFs and 1° for the rotary DOFs.

For the position controller, proportional and derivative gains were chosen differently for the translational and the rotary DOFs. The translational gains were chosen as $P_t = 2500\,\text{N/m}$ and $D_t = 60\,\text{Ns/m}$, the rotary gains as $P_r = 2000\,\text{Nm/rad}$ and $D_r = 20\,\text{Nms/rad}$. The forgetting factor f_f was set to 0.2, $\bar{P}$ and $\bar{D}$ both to 20.

The measurement of the user's center of mass was evaluated with the same amount of additional weights (80 kg) which were mounted once centrically on the mattress and once with an offset of 10 cm in lateral (x) direction. The position of the center of mass was measured in static and dynamic conditions. In the latter condition, the bed moved along various translational and rotational sinusoidal trajectories with a frequency of 0.3 Hz.

5. Results

5.1. Robot model

5.1.1. Friction model. The friction components of the motorized drum and the deflection unit were both identified with the proposed method; the torque introduced by the friction in the motorized drum is approximately three times as large as the friction in the deflection unit.

5.1.2. Measurement of user position. The measurement with the centered weight lead to a measurement result of –0.01 m for the x-value of the center of mass, while the platform hung in the stationary pose 0.5 m above ground. When the platform moved in the z-direction, the value started to oscillate with an average value of 0 m (Fig. 14(a)). In case of the displaced payload weights (offset of –0.1 m), the results show an x-value of the center of mass of –0.09 m during the stationary condition. During the movement in the z-direction, the value again slightly oscillated with an average of –0.10 m (Fig. 14(b)). Further measurements showed that

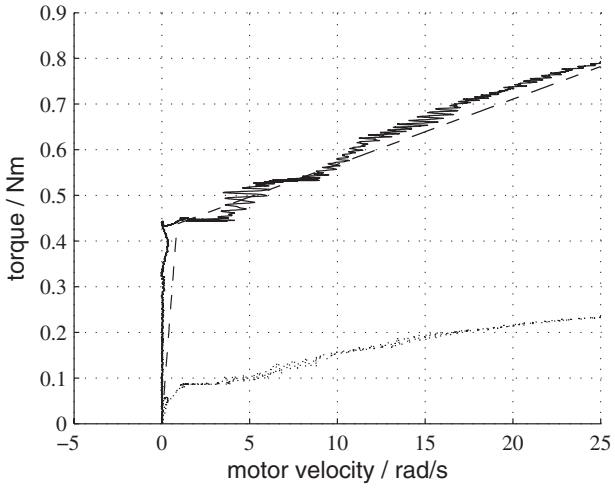

Fig. 13. Friction-velocity correlation of the drive train ($r_D = 37.5$ mm; solid line: overall friction; dotted line: friction of deflection unit; dashed line: function for model-based friction compensation).

the amplitudes of these oscillations depend on the platform movement, but the average value remains at the correct value.

5.2. Position control

The position controllers of the 3D applications, rowing and tennis, showed similar performances (Table 6). The mean error and the standard deviation are in the same order of magnitude. For both applications, the performance values satisfied the requirements defined by the conductors of the studies.

When the user interfered with the oar in the rowing application, the mean error hardly changed although interaction forces of up to 107 N were reached. The maximal position error stayed in the same order of magnitude as well (4.5 cm without, and 5.16 cm with interaction of the user). Regarding the solid angle of the oar, the error reached values of 0.65° (standard deviation 0.37°) with user interference.

The parallel structure of the r^3-system results in movement errors on all axes, also when the end effector is moved along/around a single body axis. In case of the Somnomat, the interference between the movement axis and the remaining axes is analyzed in terms of maximal position error (Table 6.3). It can be observed that the control error of the axis whose desired position is changing, is in most cases larger than on the axes whose desired position is kept constant. The movement errors depend on the axis being moved. The maximum errors reach high values for translational movements along the y-axis and the z-axis. The error on the rotary axes stays small for all conditions.

6. Discussion

In this section, we want to discuss in how far the r^3-system meets the overall project requirements to develop a versatile reconfigurable haptic interface for research on human reaction to multi-modal stimulation in a VR environment. Consequently, the used control scheme, the robot model, and the performance achieved on the three applications will be analyzed.

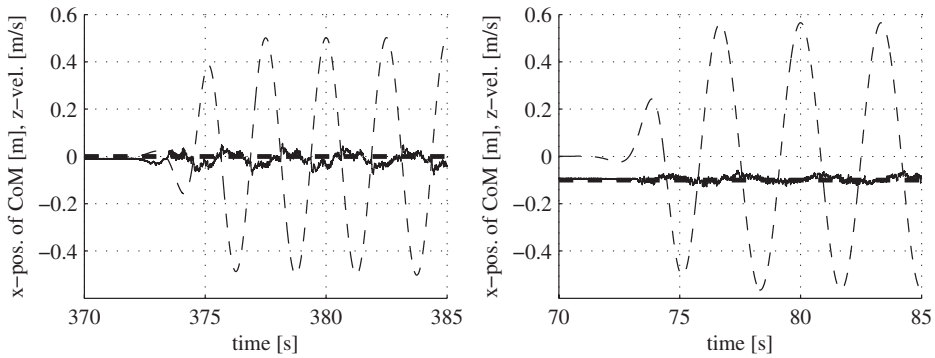

Fig. 14. Measured x-position of the center of mass (solid line) during vertical movement of the platform (dashed line: desired velocity): with weights fixed centrically (a) and with a negative x-offset of 0.1 m (bold dashed line: actual weight position) (b).

Table I. Errors of the position controller for rowing and tennis (mean and standard deviation).

	mean error (sd) [mm]
Rowing w/o user	25 (12)
Rowing with user	25 (12)
Tennis w/o user	12 (6)

6.1. The r³-system as a versatile reconfigurable haptic interface

The drive train of the r³-system was developed to meet the demanding requirements on a haptic display for sports simulation. Regarding achievable dynamics and signal processing, all requirements were met. Furthermore, the robot was successfully integrated in the CAVE environment.

As the r³-system was developed as a versatile multi-functional haptic interface, its user-friendly reconfigurability is an essential evaluation criteria. For the hardware, an experienced person needs two to three days to setup a new application, depending on its complexity. On the software side, the development of task-specific functions or algorithms might be necessary, as shown in case of the Somnomat. However, the basic control concept can be reused for all applications.

6.2. Analysis of the robot configurations chosen

As ropes only impose unidirectional constraints, the full control of n DOFs requires $m > n$ ropes.[44] Hence, for a 3-DOF task like rowing and tennis, at least four ropes are required. However, a higher number of ropes m is used ($m = 5$ for rowing and $m = 6$ for tennis). This is necessary because of the unfavorable position and size of the workspace. By increasing the number of ropes, the workspace size and the robot wrench were both increased to meet the requirements.

6.3. Robot model

The two main friction components, namely the motorized drum and the deflection unit, were identified and quantified. Identification was only performed for one load and one deflection angle around the deflection unit, however. To get a more comprehensive friction model, an extensive measurement protocol involving different loads and deflection angles is necessary. Except for the drum radius, this model does not require any task-specific adaptations.

In contrast, the end-effector model had to be extended in case of the Somnomat by the model of the counterweights. This extension is important, as the counterweights contribute one-third of the total moved mass of the system. A further significant non-linearity is introduced by the possible movement of the user's center of mass on the Somnomat platform. A restriction of the user's movement is not possible, as it is not conform with the requirements of the planned study. It was shown that these movements can be monitored online using the force sensors of the system and the inverse robot model. When starting oscillatory movements, the calculation of the center of mass is influenced by model uncertainties, e.g. resulting from relative movement between the payload masses and the mattress, partially uncompensated friction or similar. However, the mean of the oscillating value is at the actual position of the center of mass. Therefore, the correct value could be extracted by using a high-order moving average filter or a similar filter, as the sleeping subject is not supposed to change his position continuously. In this case, the measurement cannot only be used as a safety feature, but also for model-based compensation of the wrench introduced by the user's displacement in the future.

6.4. Controller performance

It was a major objective of the project to develop and use controllers which require minimal task-specific adaptations. In pre-tests, the simplest control strategies, such as classical PD position control and open-loop force control, did not show satisfactory performance. The model-based compensation of the non-linear disturbances resolved this problem and can be adapted with relatively small effort to different tasks. The implementation effort is extended if a complex end effector, e.g., the Somnomat platform with mechanical mass compensation, is used

The controller gains were set experimentally. A global rule for this setting cannot be given due to large differences of the three applications and their non-linear behavior. Especially the Somnomat has to be regarded as a highly time-variant

Table II. Mean position error of the Somnomat (standard deviation in parentheses; bold: position error of the moved axis; all other values in the same line are position errors of the remaining movement axes whose reference position is held at a constant value).

	Δx	Δy	Δz	$\Delta\phi$	$\Delta\delta$	$\Delta\psi$
x-movement	**–1 (5)** mm	–5 (2) mm	2 (5) mm	0.2 (0.2)°	0.2 (0.8)°	0.0 (0.3)°
y-movement	–1 (1) mm	**7 (11)** mm	7 (6) mm	0.3 (0.5)°	0.1 (0.0)°	0.0 (0.2)°
z-movement	–1 (1) mm	–5 (3) mm	**3 (12)** mm	0.2 (0.1)°	0.2 (0.1)°	0.0 (0.0)°
ϕ-movement	–1 (1) mm	–7 (8) mm	9 (1) mm	**0.1 (0.3)**°	0.1 (0.0)°	0.0 (0.1)°
δ-movement	–1 (9) mm	–5 (1) mm	–3 (4) mm	0.0 (0.3)°	**0.1 (0.5)**°	0.0 (0.4)°
ψ-movement	–1 (8) mm	1 (0) mm	5 (1) mm	0.2 (0.1)°	0.1 (0.2)°	**0.0 (0.4)**°

plant, as the possible user movement on the platform can lead to different rope loads at the same pose. However, an interesting globally applicable finding concerning stability could be made: When only the minimal number of ropes (equal to the number of DOFs) was used for the kinematic calculations, the system became completely uncontrollable in certain directions. In contrast, the integration of all measured rope lengths into the physics-based forward kinematics[24] resulted in stable behavior.

Despite the very different trajectories and loads, position errors stayed below the admissible errors in case of both 3D-applicaions, rowing, and tennis. For the Somnomat, the admissible position errors were exceeded for some movements on the translational axes. With slight adaptations of the model parameters depending on the movement axis, the desired accuracy was reached on these axes.

The quality of the controller is affected by the static friction in the system. In this context, low friction of the deflection units is important: As these units are placed between the tensionmeters and the end effector, friction leads to measurement errors. Therefore, the static friction in the deflection units should be minimized.

7. Conclusion and Outlook

Systematic research on human body reaction in a multimodal VR environment requires a highly versatile haptic interface. Moreover, if the research focus is set on the field of sports, the demands on the haptic interface are further increased. Already from an overall perspective on available robots, elevated forces as they are applied in rowing or the high velocities and accelerations performed during a tennis stroke are demanding requirements. Hence, the development of a haptic interface planned as an overall tool for research on motor learning in sports is a challenging task in many respects, from the overall versatility to the application-specific adaptability.

The tendon-based r^3-system turned out to be a feasible approach regarding both versatility and adaptability. In this context, the most important key features are that the deflection points can be almost freely positioned, that the transmission rate can be changed with little hardware effort, and that the control software contains a high number of reusable sub-functions. The visual and auditory displays are hardly influenced by the r^3-system as the ropes do not impair the user's vision and the actuators, as the main noise-producing units, are placed outside the CAVE. The r^3-system is a unique haptic interface regarding the size of its workspace, the achievable dynamics in terms of velocity, acceleration, and forces, as well as its versatility.

The implemented controller fulfilled the requirements in the 3D applications without further adaptations. On the Somnomat, the integration of an ILC increased the performance significantly; mainly, unwanted rotations were suppressed. For the next study, a parameter set will be searched which improves the performance on the translational axes while maintaining the accuracy on the rotary axes. In this context, a thorough stability analysis is planned for the Somnomat which includes the eigenfrequencies of the system in different directions, depending on the user position on the platform.

All three setups could be successfully used for user studies in the meantime: On the Somnomat, a pre-study with three subjects and movement in all degrees of freedom between 0.4 and 2 Hz was performed.[45] Additionally, positions for the rotary axes as well as combined rotations were tested. As the high-frequent movements were rated as unpleasant, only movements with frequencies around 0.4 Hz as they were validated in this paper will be considered for future studies. On the rowing simulator, the efficiency of various haptic feedback strategies including simple position control was tested on nine subjects. Recently, a similar study involving 21 subjects was successfully finished on the tennis setup.

Acknowledgments

The authors would like to thank Andreas Brunschweiler, Dr. Peter Wolf, Dr. Alexander Duschau-Wicke, and Dr. Heike Vallery for their contributions to this work. This work was supported by local sources of ETH Zurich. Laura Marchal-Crespo receives a scholarship from the Fundacion Caja Madrid.

References

1. R. Ham, T. Sugar, B. Vanderborght, K. Hollander and D. Lefeber, "Compliant actuator designs," *IEEE Robot. Autom. Mag.* **16**(3), 81–94 (Sept. 2009).
2. H. Vallery, J. Veneman, E. van Asseldonk, R. Ekkelenkamp, M. Buss and H. van Der Kooij, "Compliant actuation of rehabilitation robots," *IEEE Robot. Autom. Mag.* **15**(3), 60–69 (Sept. 2008).
3. L. Marchal-Crespo and D. Reinkensmeyer, "Review of control strategies for robotic movement training after neurologic injury," *J. NeuroEngineering and Rehabil.* **6**(1), 20 (2009).

4. R. Riener, A. Duschau-Wicke, A. König, M. Bolliger, M. Wieser and H. Vallery, "Automation in Rehabilitation: How to Include the Human into the Loop," *World Congress on Medical Physics and Biomedical Engineering, September 7 - 12, 2009, Munich, Germany*, volume 25/13 of *IFMBE Proceedings* (R. Magjarevic, O. Dössel and W. C. Schlegel, eds.), (Springer Berlin Heidelberg, 2009) pp. 180–183.
5. A. Koenig, D. Novak, X. Omlin, M. Pulfer, E. Perreault, L. Zimmerli, M. Mihelj and R. Riener, "Real-time closed-loop control of cognitive load in neurological patients during robot-assisted gait training," *IEEE Trans. Neural Syst. Rehabil. Eng.* **19**(4), 453–464 (Aug. 2011).
6. J. L. Andreassi, *Psychophysiology: Human Behavior and Physiological Response* (Lawrence Erlbaum Assoc Inc, 2006).
7. C. M. Welch, S. A. Banks, F. F. Cook and P. Draovitch, "Hitting a baseball: A biomechanical description," *J. Orthopaedic and Sports Physical Therapy* **22**, 193–193 (1995).
8. R. E. Bahamonde and D. Knudson, "Kinetics of the upper extremity in the open and square stance tennis forehand," *J. Sci. Med. Sport.* **6**(1), 88–101 (2003).
9. S. Plagenhoef, *Patterns of Human Motion: A Cinematographic Analysis* (Prentice-Hall Englewood Cliffs, NJ, 1971).
10. J. M. Steinacker, W. Lormes, M. Lehmann and D. Altenburg, "Training of rowers before world championships," *Med. Sci. Sports & Exercise*. **30**(7), 1158 (1998).
11. D. Cabrera, A. Ruina and V. Kleshnev, "A simple 1+ dimensional model of rowing mimics observed forces and motions," *Hum. Mov. Sci.* **25**(2), 192–220 (2006).
12. T. H. Massie and J. K. Salisbury, "The Phantom Haptic Interface: A Device for Probing Virtual Objects," *Proceedings of the ASME Winter Annual Meeting, Symposium on Haptic Interfaces for Virtual Environment and Teleoperator Systems*, Chicago, IL (Nov. 1994) vol. 1, pp. 316–317.
13. S. Grange, F. Conti, P. Rouiller, P. Helmer and C. Baur, "The delta haptic device," *Mecatronics 2001* (2001).
14. E. Colgate and N. Hogan, "An Analysis of Contact Instability in Terms of Passive Physical Equivalents," *Proceedings of the IEEE International Conference on Robotics and Automation*, IEEE, Scottsdale, AZ (May 1989) pp. 404–409.
15. M. Wellner, R. Sigrist and R. Riener, "Virtual competitors influence rowers," *PRESENCE: Teleoperators and Virtual Environments*. **19**(4), 313–330 (2010).
16. D. A. Lawrence, L.Y. Pao, A. C. White and W. Xu, "Low Cost Actuator and Sensor for High-Fidelity Haptic Interfaces," *Proceedings of the 12th International Symposium on Haptic Interfaces for Virtual Environment and Teleoperator Systems*, Chicago, IL (March 2004) pp. 74–81.
17. O. R. Astley and V. Hayward, "Design Constraints for Haptic Surgery Simulation," *IEEE International Conference on Robotics and Automation, 2000. Proceedings. ICRA'00*, San Francisco, CA (Apr. 2000) vol. 3, pp. 2446–2451.
18. D. A. Lawrence, L. Y. Pao and S. Aphanuphong, "Bow Spring/Tendon Actuation for Low Cost Haptic Interfaces," *First Joint Eurohaptics Conference and Symposium on Haptic Interfaces for Virtual Environment and Teleoperator Systems*, Pisa, Italy (March 2005) pp. 157–166.
19. R. Riener, L. Lünenburger, I. C. Maier, G. Colombo and V. Dietz, "Locomotor training in subjects with sensory-motor deficits: An overview of the robotic gait orthosis lokomat," *J. Healthc. Eng.* **1**(2), 197–216 (2010).
20. R. Wilson and G. Niemeyer, "Motion Control of Impedance-Type Haptic Devices," *Proceedings of the IEEE International Conference on Robotics and Automation, ICRA '09*. Kobe, Japan (May 2009) pp. 1092–1097.
21. J.-P. Merlet and D. Daney, "A New Design for Wire-Driven Parallel Robot," *Proceedings of the Design and Modelling of Mechanical Systems, 2nd World Congress*, Monastir, Tunisia (March 2007).
22. J. von Zitzewitz, G. Rauter, R. Steiner, A. Brunschweiler and R. Riener, "A Versatile Wire Robot Concept as a Haptic Interface for Sport Simulation," **In**: *Proceedings of the 2009 IEEE International Conference on Robotics and Automation (ICRA)*, Kobe, Japan (12–17 May 2009) pp. 313–318.
23. J.-P. Merlet, "Marionet, a Family of Modular Wire-Driven Parallel Robots," **In**: *Advances in Robot Kinematics: Motion in Man and Machine* (J. Lenarcic and M. M. Stanisic, eds.) (Springer Netherlands, 2010) pp. 53–61.
24. J. von Zitzewitz, G. Rauter, H. Vallery, A. Morger and R. Riener, "Forward Kinematics of Redundantly Actuated, Tendon-Based Robots," *Proceedings of the IEEE/RSJ International Conference on Intelligent Robots and Systems, IROS '10*, Taipei, Taiwan (Oct. 2010) pp. 2289–2294.
25. M. Bouri, B. Le Gall and R. Clavel, "A New Concept of Parallel Robot for Rehabilitation and Fitness: The Lambda," *Proceedings of the IEEE International Conference on Robotics and Biomimetics (ROBIO)*, Guilin, China (Dec. 2009) pp. 2503–2508.
26. D. Mayhew, B. Bachrach, W. Z. Rymer and R. F. Beer, "Development of the MACARM - A Novel Cable Robot for Upper Limb Neurorehabilitation," *Proceedings of the 9th International Conference on Rehabilitation Robotics, ICORR*, Chicago, IL (June/July 2005) pp. 299–302.
27. EtherCAT Technology Group, "Ethercat - the ethernet fieldbus. http://www.ethercat.org/en/technology.html (March 2011).
28. J. von Zitzewitz, P. Wolf, V. Novakovic, M. Wellner, G. Rauter, A. Brunschweiler and R. Riener, "A real-time rowing simulator with multi-modal feedback," *Sports Technol.* **1**(6), 257–266 (2009).
29. G. Rauter, R. Sigrist, L. Marchal-Crespo, H. Vallery, R. Riener and P. Wolf, "Assistance or Challenge? Filling a Gap in User-Cooperative Control," *Proceedings of the IEEE/RSJ International Conference on Intelligent Robots and Systems, IROS 2011*, San Francisco, CA (Sep. 2011).
30. C. R. Carignan and K. R. Cleary, "Closed-loop force control for haptic simulation of virtual environments," *Haptics-e*. **1**(2), 1–14 (2000).
31. S. Jezernik, G. Colombo, T. Keller, H. Frueh and M. Morari, "Robotic orthosis lokomat: A rehabilitation and research tool," *Neuromodulation*. **6**(2), 108–115 (2003).
32. S. Fang, *Design, Modeling and Motion Control of Tendon-Based Parallel Manipulators* (VDI Fortschritt-Bericht, 2005).
33. H. J. Ferreau, P. Ortner, P. Langthaler, L. del Re and M. Diehl, "Predictive control of a real-world diesel engine using an extended online active set strategy," *Annu. Rev. Control*. **31**(2), 293–301 (2007).
34. R. Verhoeven, Analysis of the Workspace of Tendon-Based Stewart Platforms *Ph.D. thesis* (Duett, Universitätsbibliothek Duisburg, 2004).
35. G. Rauter, J. von Zitzewitz, A. Duschau-Wicke, H. Vallery and R. Riener, "A Tendon-Based Parallel Robot Applied to Motor Learning in Sports," *Proceedings of the 3rd IEEE RAS and EMBS International Conference on Biomedical Robotics and Biomechatronics, BioRob 2010*, Tokio, Japan (Sep. 2010) pp. 82–87.
36. G. R. Reding and C. Fernandez, "Effects of vestibular stimulation during sleep," *Electroencephalogr. Clin. Neurophysiol.* **24**(1), 75–79 (1968).
37. G. M. Jones and N Sugie, "Vestibulo-ocular responses in man during sleep," *Electroencephalogr. Clin. Neurophysiol.* **32**(1), 43 (1972).
38. E. S. Tauber, G. Handelman, R. Handelman and E. D. Weitzman, "Vestibular stimulation during sleep in young adults," *Arch. Neurol.* **27**(3), 221–228 (Sep 1972).
39. E. M. Ornitz, A. B. Forsythe and A. De la Pea, "The effect of vestibular and auditory stimulation on the rapid eye movements of rem sleep in normal children," *Electroencephalogr. Clin. Neurophysiol.* **34**(4), 379–390 (Apr 1973).

40. S. Woodward, E. S. Tauber, A. J. Spielmann and M. J. Thorpy, "Effects of otolithic vestibular stimulation on sleep," *Sleep*. **13**(6), 533–537 (Dec. 1990).
41. I. Constantinescu, L. Bayer, S. Perrig, P. Vidal, M. Muhlethaler and S. Schwartz , "Rock to sleep: The impact of gentle rocking on an afternoon nap," *Eurpean Sleep Res. Soc*., Lisbon, Portugal (Sep. 2010).
42. K. L. Moore, *Iterative Learning Control for Deterministic Systems* (Springer-Verlag New York, Inc. Secaucus, NJ, USA, 1993).
43. A. Duschau-Wicke, J. von Zitzewitz, R. Banz and R. Riener, "Iterative Learning Synchronization of Robotic Rehabilitation Tasks," *Proceedings of the IEEE 10th International Conference on Rehabilitation Robotics, ICORR 2007*, IEEE, Noordwijk, the Netherlands (June 2007) pp. 335–340.
44. S. Kawamura, M. Ida and T. Wada, "Development of a Virtual Sports Machine using a Wire Drive System - A Trial of Virtual Tennis," *Proceedings of the IEEE/RSJ International Conference on Intelligent Robots and Systems*, Pittsburgh (1995) pp. 111–116.
45. X. Omlin, J. von Zitzewitz, G. Rauter, A. Morger and R. Riener, "Robot-Driven Platform to Investigate Effects of Vestibular Stimulation on Sleep," *Proceedings of the 19th Annual Meeting of the German Society for Sleep Research and Sleep Medicine*, Mannheim, Germany (November 2011).